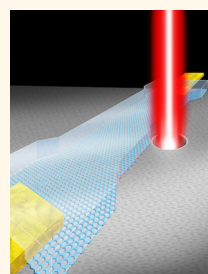


Toward Sensitive Graphene Nanoribbon–Nanopore Devices by Preventing Electron Beam-Induced Damage

Matthew Puster,^{†,*,§} Julio A. Rodríguez-Manzo,^{†,§} Adrian Balan,^{†,§} and Marija Drndić^{†,*}

[†]Department of Physics and Astronomy, University of Pennsylvania, Philadelphia, Pennsylvania 19104, United States and [‡]Department of Materials Science and Engineering, University of Pennsylvania, Philadelphia, Pennsylvania 19104, United States. [§]M. Puster, J. A. Rodríguez-Manzo, and A. Balan contributed equally to this work.

ABSTRACT Graphene-based nanopore devices are promising candidates for next-generation DNA sequencing. Here we fabricated graphene nanoribbon–nanopore (GNR-NP) sensors for DNA detection. Nanopores with diameters in the range 2–10 nm were formed at the edge or in the center of graphene nanoribbons (GNRs), with widths between 20 and 250 nm and lengths of 600 nm, on 40 nm thick silicon nitride (SiN_x) membranes. GNR conductance was monitored *in situ* during electron irradiation-induced nanopore formation inside a transmission electron microscope (TEM) operating at 200 kV. We show that GNR resistance increases linearly with electron dose and that GNR conductance and mobility decrease by a factor of 10 or more when GNRs are imaged at relatively high magnification with a broad beam prior to making a nanopore. By operating the TEM in scanning TEM (STEM) mode, in which the position of the converged electron beam can be controlled with high spatial precision *via* automated feedback, we were able to prevent electron beam-induced damage and make nanopores in highly conducting GNR sensors. This method minimizes the exposure of the GNRs to the beam before and during nanopore formation. The resulting GNRs with unchanged resistances after nanopore formation can sustain microampere currents at low voltages (~50 mV) in buffered electrolyte solution and exhibit high sensitivity, with a large relative change of resistance upon changes of gate voltage, similar to pristine GNRs without nanopores.



KEYWORDS: DNA · sequencing · graphene nanoribbon · nanopore · silicon nitride · TEM · STEM

Graphene is a uniquely qualified material for nanopore-based DNA sequencing. It is one atom thin—as thin as an individual DNA base—and has low electrochemical reactivity when operated in buffered solutions.¹ As a zero-gap semimetal with high conductivity, graphene exhibits an ambipolar field effect with high mobilities for both electrons and holes² and is very sensitive to the local electrostatic potential, showing single-molecule detection at room temperature.³ Graphene structures can be positioned and patterned *via* electron-beam lithography and oxygen plasma etching to form graphene nanoribbons (GNRs)^{4,5} and nanoconstrictions.^{6,7} Alternatively, formation of graphene structures by transmission electron beam ablation lithography (TEBAL)⁸ affords the most precise control of device width, enabling graphene structures down to a few nanometers in width,⁹ which can sustain microampere currents.¹⁰

Graphene nanoribbon–nanopore (GNR-NP) sensors have been proposed for DNA sequencing.^{11–14} The mechanism suggested to sequence DNA relies on measuring the modulation of current flowing through a GNR induced by each base in an unlabeled single-stranded DNA molecule as it passes through a nanopore in or next to that GNR. The atomic structure of each nucleotide is expected to result in a unique electrostatic potential that will modulate the charge density in the surrounding narrow GNR, causing a modulation of its measured conductance. This effect is much like the operation of a field effect transistor, where the potential applied to the gate modulates the charge density in the semiconducting channel and alters the current flowing through the transistor. Standard currents sustained by GNRs (~1 μ A) are orders of magnitude higher than standard ionic currents (~0.1–10 nA) passing through nanopores; thus GNRs are expected to yield

* Address correspondence to drndic@physics.upenn.edu.

Received for review September 29, 2013 and accepted November 13, 2013.

Published online
10.1021/nn405112m

© XXXX American Chemical Society

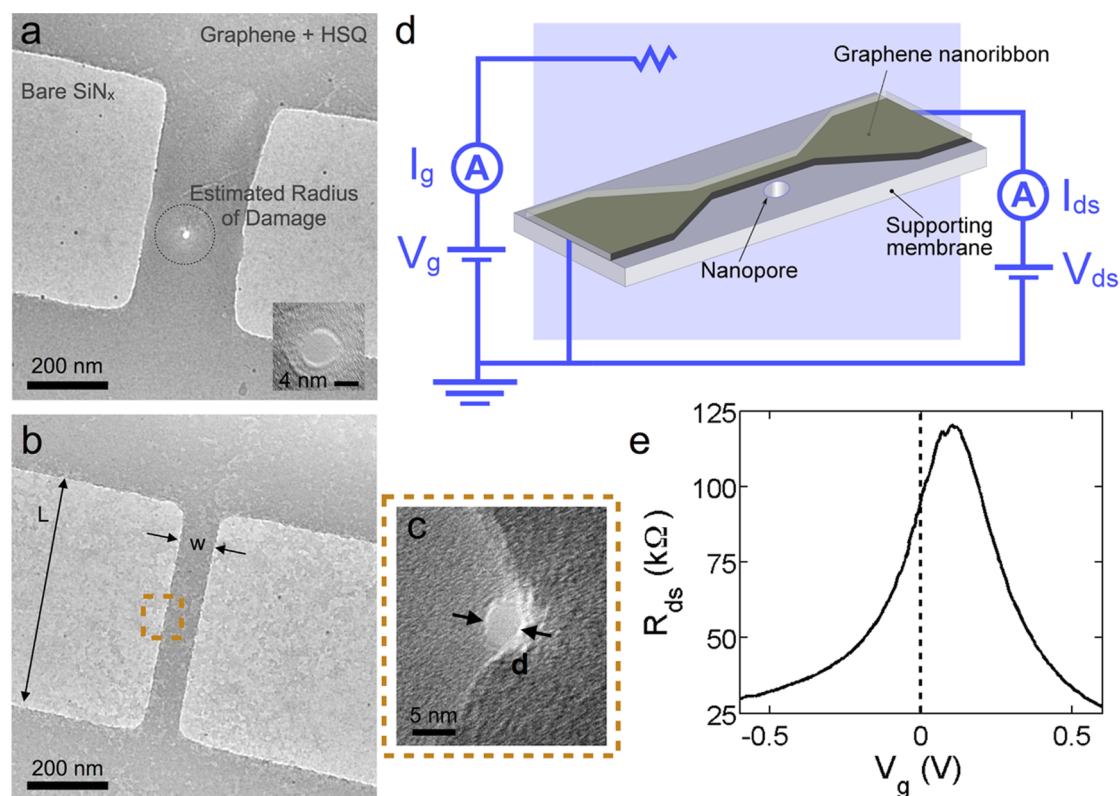


Figure 1. Single-layer graphene nanoribbon–nanopore device. (a–c) TEM images of GNR devices. The dark gray areas are graphene covered with a 15 nm thick layer of hydrogen silsesquioxane (HSQ). Light gray areas are the bare 40 nm thick supporting silicon nitride (SiN_x) membrane. (a) Nanopore formed in the center of the GNR ($L = 600$ nm, $w = 240$ nm) by converging the electron beam in TEM mode. The black circle indicates a damaged region within a radius of ~ 75 nm; however, that damage is not visible in the TEM image. Inset of (a): High-magnification TEM image of the nanopore ($d = 7$ nm). (b) GNR ($L = 600$ nm, $w = 85$ nm) prior to nanopore drilling. (c) Nanopore ($d = 4$ nm) formed next to a GNR. (d) Schematic showing the GNR-NP device and the circuit diagram used for electrolytic gating in KCl solution. (e) GNR resistance (R_{ds}) vs gate voltage (V_g) during electrolytic gating of a GNR before nanopore formation.

higher signal-to-noise ratio and sequencing speeds with a potential to read at 10 MHz bandwidths, *i.e.*, 10 million bases per second, for genome sequencing in 15 min. However, GNR-NP devices have yet to be realized. Theoretical models assume suspended GNRs with nanopores, precise edge structure, and no electrolyte solution or screening.^{11,13,14} Practical realization requires GNR-NPs to be supported on substrates, at least partially along the edges, and GNR edge structure is not likely to be well-defined. DNA-induced conductance modulations in silicon nanowires were observed by Xie *et al.*,^{15,16} and the model they develop predicts a decay in perturbing potential with distance from the nanopore. A calculation based on this model is included in Figure S1. Compared to such sensors, GNRs offer the potential for better spatial resolution and higher change in device conductance due to nearby molecules.

In this paper we report the fabrication and electrical characterization of GNR-NP sensors (Figure 1) for biomolecule detection and analysis, measurements of GNR conductance *during* nanopore formation, and a methodology for preventing electron beam-induced damage to GNRs. We also show how different procedures

used for nanopore formation in the TEM affect the gating response of GNR-NP sensors.

RESULTS AND DISCUSSION

Nanopores with diameters ranging from 2 to 10 nm were formed with a converged TEM electron beam at the edges or in the center of 20–250 nm wide, 600 nm long GNRs, fabricated in 40 nm thick silicon nitride membranes. GNRs were patterned from CVD-grown single-layer graphene using electron-beam lithography on negative-tone resist hydrogen silsesquioxane (HSQ, Dow Corning XR-1541, 2%)^{17,18} and oxygen plasma etching, resulting in GNRs sandwiched between the SiN_x membrane and the HSQ etch mask. Figure 1 shows TEM images of a 240 nm wide GNR with a 7 nm diameter nanopore in the center of the GNR (Figure 1a), an 85 nm wide GNR prior to making a nanopore (Figure 1b), and a 4 nm diameter nanopore formed at the edge of a GNR (Figure 1c). The GNR is visible in TEM because of the ~ 15 nm thick HSQ protective layer serving as the etch mask that has been left on top of the graphene. The thickness of the HSQ etch mask was confirmed by atomic force microscopy (AFM) height measurements (Figure S2). Details of

the CVD-grown graphene (electron diffraction, Raman spectra, etc.) and device fabrication are given in the Methods and Supporting Information sections. Additional TEM images of fabricated GNRs of different widths down to 20 nm and GNRs with side gates are shown in Figures S3, S4, and S5.

To characterize the gating response in a realistic electrochemical environment, the GNR-NP devices fabricated here were immersed in 1 M KCl, and a gate voltage (V_g) was applied to a Ag/AgCl solution electrode while the resistance (R) of the GNR was measured (Figure 1d). The GNR sensors are most sensitive to external potentials at gate voltages where the R vs V_g curve is the steepest. The GNR resistance exhibits a maximum, *i.e.*, the charge neutrality point, at $V_g \approx 140$ mV (Figure 1e). The shift in the charge neutrality point from $V_g = 0$ V, for undoped graphene, to 140 mV indicates that the graphene is p-doped, most likely due to doping from residues left from processing.^{19–21} For this device shown in Figure 1e, a perturbation of the potential near the ribbon of ~ 10 mV should generate a ~ 60 nA change in GNR current from a baseline current of $1.5 \mu\text{A}$, a variation large enough for measurements at high frequency (>1 MHz).

Making the nanopore with the converged electron beam is the last step in our device fabrication process. While there are other ways to make nanopores,^{22,23} to our knowledge this is still the best way to make the smallest nanopores.²⁴ Alternatively, nanopores could be made prior to GNR fabrication, but this method creates other challenges of precise alignment, scalability, and nanopore filling or closing. The main challenge of creating nanopores next to GNRs using an electron beam is that, to precisely locate the position for nanopore drilling relative to the GNR, it is necessary to image some part of the device at relatively high magnification and thus high current densities. The 200 keV electron beam energy is high enough to damage graphene,^{25,26} so the exposure of the GNR to the beam must be kept to a minimum.

To define optimal conditions to form a nanopore without damaging the GNR, we measured the electron beam-induced damage in GNRs for different imaging conditions, namely, transmission electron microscopy (TEM) and scanning TEM (STEM) modes. In particular, we measured *in situ* the change in resistance of GNRs in a two terminal configuration as a function of electron dose using a TEM sample holder equipped with electrical feedthroughs (Hummingbird Scientific). Figure 2a shows an optical image of the TEM sample holder (left panel) and optical and scanning electron microscope (SEM) images of the device (right panel).

In TEM imaging mode we observed an irreversible and linear increase in GNR resistance with electron irradiation time for imaging conditions used to locate the GNR edge, *even prior* to fully condensing the beam to form the nanopore (Figure 2b). In this mode, the

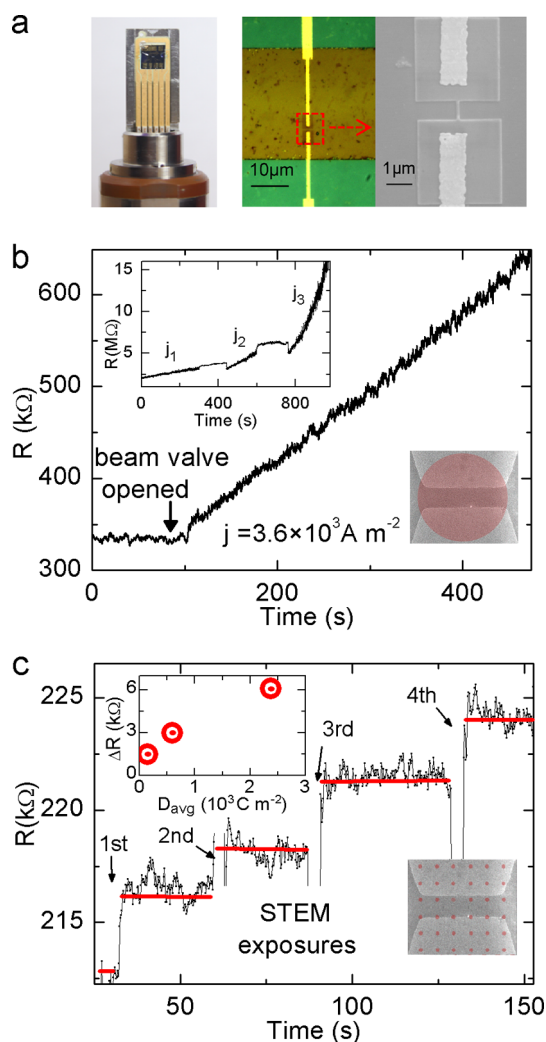


Figure 2. *In situ* electrical measurement of the GNR resistance upon exposure to TEM and STEM imaging conditions. (a) Optical image of *in situ* TEM sample holder showing a chip with GNR-NP devices. Right panel: Optical image showing Au electrodes leading to a GNR-NP device on top of a SiN_x membrane together with a magnified SEM image of the highlighted rectangle. (b) *In situ* TEM electrical measurement of GNR resistance vs time for broad-beam TEM imaging. Upon exposure of the GNR at $j = 3.6 \times 10^3 \text{ A m}^{-2}$ (indicated as “beam valve opened”) the resistance increases linearly with time. Top-left inset of (b): The rate of change of resistance increases with current density (j_1 , j_2 , and j_3 are 3, 9, and $23 \times 10^4 \text{ A m}^{-2}$, respectively). Bottom-right inset of (b): Illustration of a GNR exposed to a broad beam (red circle) in TEM imaging mode. (c) *In situ* STEM electrical measurement of GNR resistance vs time for converged beam STEM imaging. GNR resistance increases in a step-like fashion after each 330 ms scan in between the four steps, indicated by arrows. Top-left inset of (c): Average increase of resistance (ΔR) per STEM scan exposure as a function of average dose (D_{av}). Bottom-right inset of (c): Illustration of the STEM scan over a GNR. The array of red spots simulates the position of the beam over different pixels.

spread electron beam continuously irradiates a broad area of the sample under observation, illustrated by a large red circle in the inset of Figure 2b. The increase in resistance of the GNRs is due to the creation of defects in the graphene.^{27,28} For graphene, resistance scales

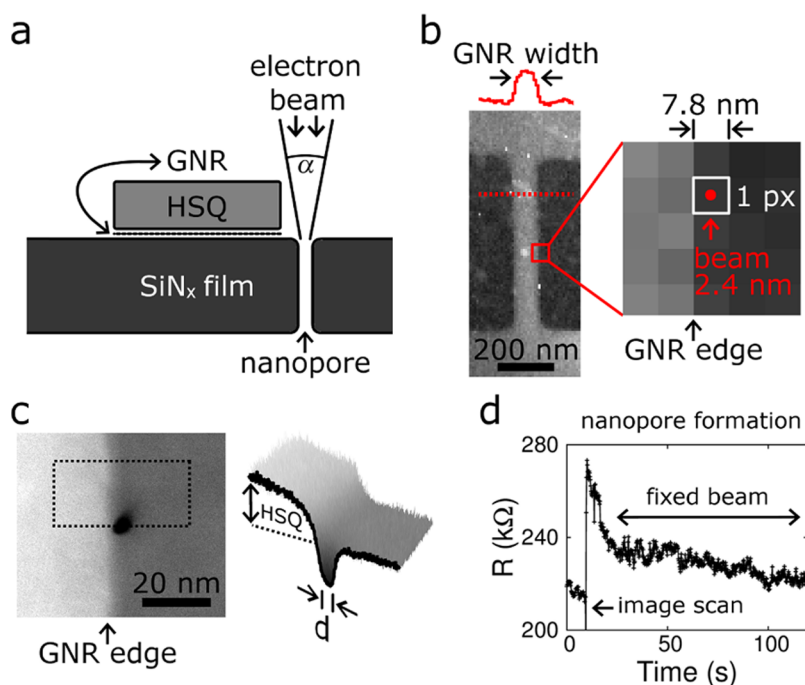


Figure 3. Formation of nanopores in STEM mode to avoid electron beam-induced damage in GNRs. (a) Diagram showing a cross-section of a device with a nanopore in a SiN_x membrane next to a GNR, and the converged electron beam at the nanopore position (diagram not to scale). (b) HAADF STEM image showing a 100 nm wide GNR. The image was taken with a 2.4 nm beam diameter ($j = 0.4 \times 10^9 \text{ A m}^{-2}$), a 7.8 nm pixel size, and a $5 \mu\text{s}$ dwell time per pixel. Therefore, each pixel received a dose of $2 \times 10^3 \text{ C m}^{-2}$. The inset shows that the contrast provided by the HSQ mask allows positioning of the beam at the edge of the GNR with a precision of $\sim 4 \text{ nm}$. The red dot (2.4 nm in diameter) shows the spatial relationship between the beam and the pixel size of the image. (c) High-resolution HAADF STEM image of a nanopore next to a GNR (the image was taken with a 0.3 nm beam diameter). The right panel shows a perspective view of the image enclosed by the highlighted rectangle. From these intensity profiles it is possible to calculate the nanopore diameter (d) and the length between the nanopore and the GNR. (d) Resistance of a GNR during nanopore formation. The spike in the resistance corresponds to an image scan and is indicated by the leftmost arrow. The decay of resistance is a discharging effect. Immediately after the image was acquired the beam was fixed next to the GNR (as in (b)) and left immobile in order to form the nanopore. There is only a small change of resistance in the GNR during this process.

linearly with the density of defects, $n_d = \sigma \times D$, where σ is the displacement cross-section^{29,30} and D is the irradiation dose. The dose is defined as the product of the current density (j) and the irradiation time (t). Thus $R \approx n_d = \sigma \times D = \sigma \times t \times j$. In Figure 2b the resistance of a GNR increases linearly with time; here, the beam diameter was $1.6 \mu\text{m}$ and $j = 4 \times 10^3 \text{ A m}^{-2}$. Moreover, at higher j , the rate of change of GNR resistance increases, as shown in the inset of Figure 2b for $j = 3, 9, \text{ and } 23 \times 10^4 \text{ A m}^{-2}$. In practice, imaging at higher magnifications correlates with higher current densities. For example, at $800\times$ magnification, the GNR was continuously irradiated with a current density of $2.3 \times 10^5 \text{ A m}^{-2}$. In TEM mode, these high magnifications are needed to position the nanopore next to the GNR, and we found that the GNR is significantly damaged in a short amount of time.

In STEM mode, it is possible to image the GNR only once, with precise control over dose, in order to determine the location to form the nanopore. Figure 2c shows GNR resistance as a function of time with a step increase in resistance for each STEM image of the GNR, as indicated by arrows. The 256×256 pixel images were taken with an electron beam diameter of 2.4 nm (convergence angle $\alpha = 24 \text{ mrad}$), a current density

$j = 4 \times 10^8 \text{ A m}^{-2}$, a pixel size of 7.8 nm, and a dwell time of $5 \mu\text{s}$ per pixel. Each STEM acquisition takes 330 ms, and the constant resistance time-segments that occur immediately after each acquisition (marked with horizontal red lines in Figure 2c) show that damage occurs only during the short time when the beam scans over the GNR. In contrast to TEM mode, in the STEM mode the converged beam irradiates the sample in discrete locations, schematically depicted as the array of red spots in the inset of Figure 2c. Each discrete spot was irradiated for a total dose $D = 2 \times 10^3 \text{ C m}^{-2}$. We define an *average dose* for STEM mode as $D_{\text{av}} = D \times \text{beam area}/\text{pixel area}$. The average dose for the GNR can also be expressed as the total charge irradiating the GNR divided by the GNR surface area. For a fixed beam diameter, keeping all other parameters constant, decreasing the pixel size increases the average dose and causes a higher change in resistance (ΔR) per scan, as shown in the inset of Figure 2c. Unlike nanopore formation in the TEM method, where damage is localized in a large radius where imaging was performed prior to nanopore formation (Figure S6), any damage incurred during STEM imaging is uniform on average across the GNR, with no preference to the area around the nanopore, ensuring that the device

area close to the nanopore is just as sensitive as the rest of the device.

On the basis of our *in situ* TEM measurements from Figure 2, we developed a procedure in STEM mode to prevent beam-induced damage in GNRs during nanopore positioning and formation. The procedure involves acquiring a single image of the GNR to resolve the GNR edge, choosing a position to form the nanopore, and moving the beam to that position. The diagram of Figure 3a shows the electron beam configuration required to make a nanopore in the SiN_x film together with the neighboring GNR.

We used high-angle annular dark field (HAADF) imaging in STEM mode, where the image intensities are proportional to the mass,³¹ in order to generate high contrast in a single scan between the HSQ and SiN_x. Figure 3b illustrates the procedure. First, a single image of the GNR is acquired with the conditions used in Figure 2c. Then, a pixel at the edge of the GNR is chosen, and the beam is placed over that pixel until the pore is formed, as illustrated by the red point in the inset of Figure 3b. Typically, with these conditions, an electron dose of $D \approx 5 \times 10^{10}$ C m⁻² was enough to make a nanopore.^{32,33} In this way, the 2.4 nm diameter beam was used both to image *and* to make the nanopore in a sequential process. These imaging conditions correspond to an average dose, $D_{av} = 150$ C m⁻², a negligible number compared to the dose delivered in TEM mode, $D = 1.2 \times 10^7$ C m⁻² (60 s at $j = 2.3 \times 10^5$ A m⁻²), during typical positioning of the GNR edge before forming the nanopore. An example of a 4 nm diameter nanopore made with this procedure next to a GNR is shown in the high-resolution HAADF STEM image in Figure 3c. Figure 3d emphasizes that the GNR resistance does not change during formation of a nanopore. Any permanent damage to the GNR is incurred during the imaging prior to fixing the beam in place (provided that the nanopore is at the edge of the GNR and not in the center). A transient change in resistance was observed in both STEM and TEM modes due to charging and discharging of the SiN_x film as electrons build up and then dissipate in the film under beam irradiation. As shown in Figure 3d, the resistance recovered in the STEM mode to a value close to the original GNR resistance.

The two methods of forming pores (TEM vs STEM) are compared in Figure 4a by showing the ratios of the final and initial resistance after nanopore formation (R_f/R_i) as a function of the initial resistance (R_i) for 28 devices (11 with STEM and 17 with TEM). Following nanopore formation in TEM mode (blue squares), five out of 17 devices were nonconducting ($R_f > 10$ M Ω), while the resistance for the other devices increased on average ~ 15 times, limiting the sensitivity and maximum bandwidth. All devices narrower than 50 nm wide were nonconducting once the nanopore was formed in the TEM mode. In contrast, when nanopores

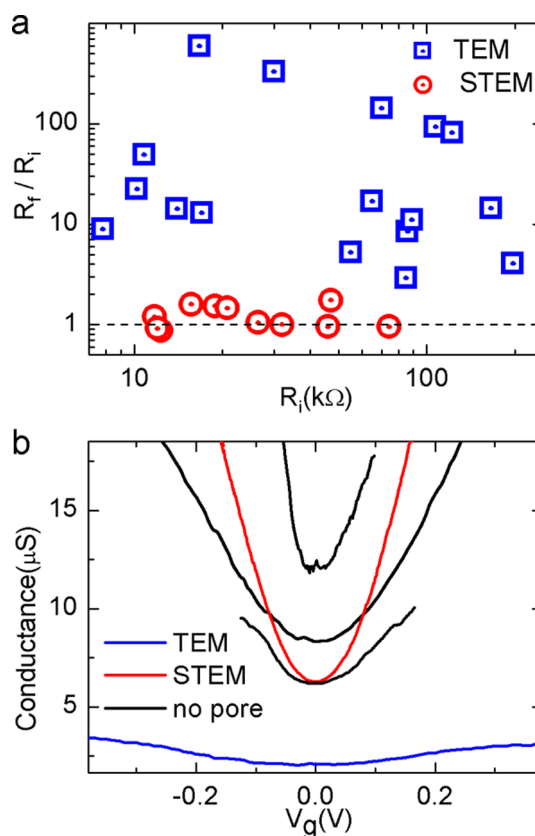


Figure 4. Comparison of GNR electrical properties after TEM and STEM nanopore formation methods. (a) Relative increase in resistance before (R_i) and after (R_f) nanopore formation for 28 GNR-NP devices made with a TEM method (17, blue squares) and STEM method (11, red circles), as a function of initial resistance, R_i . (b) GNR conductance vs gate voltage (V_g) measured in a 1 M KCl solution for representative devices before (black curves) and after nanopore formation with TEM (blue) and STEM (red) methods. For clarity, these curves were shifted so that the charge neutrality point is at $V_g = 0$ V.

were formed using the STEM technique (red circles), the resistance was effectively unchanged with $R_f/R_i \approx 1$ (see dashed line in Figure 4a), even for 50 nm wide GNRs. Bar graphs showing resistances of devices before and after nanopore formation using both methods are shown in Figure S9. The striking difference in resistance is explained by the approximately 5 orders of magnitude difference in irradiation dose on the GNR between the two methods. It is also important to note that neither current annealing after nanopore formation nor *in situ* current annealing during nanopore formation was an effective method to regain or retain the initial GNR resistance.

Figure 4b compares electrolytic gating curves (conductance vs V_g) for representative devices *before* (black curves) and *after* formation of the pore with both the STEM and TEM methods (red and blue curves, respectively). The TEM devices exhibit a significantly broader curve than the nonirradiated GNRs, with both lower conductivity and mobility, consistent with a higher density of defects.²⁷ The gating curves for STEM devices fall within the range of gating curves for devices before irradiation, conserving both conductivity and

mobility and making the STEM devices more sensitive to changes in local electric potential than those produced in TEM mode. The STEM devices show a relative change of GNR resistance with gate voltage in solution as high as $(\Delta R/R)/\Delta V_g \approx 1\%/mV$. Because of their low resistances (on the order of 10 k Ω), resulting STEM GNRs are able to sustain microampere currents at low voltages in buffered electrolyte solution.

CONCLUSIONS

In summary, we developed a sensor for single-biomolecule detection in buffered electrolyte solution consisting of nanopores in SiN_x membranes with

diameters as small as 2 nm (Figure S10) next to GNRs with widths of 20–250 nm. We prove with *in situ* TEM electrical measurements that the standard procedure of forming a nanopore next to a GNR in TEM mode exposes the GNR to an electron dose of $D \approx 10^7$ C m⁻² and significantly decreases its conductance and mobility. We developed a STEM-based method with which we can form nanopores next to the edge of a GNR, exposing the GNR to an average dose of only $D_{av} \approx 10^2$ C m⁻², 5 orders of magnitude less than the TEM method. These improved GNR-NP devices show a modulation in resistance to changes in the local potential of $\sim 1\%/mV$.

METHODS

GNR-NP fabrication starts with windows of low-stress SiN_x supported by 5 × 5 mm Si chips. The Si chips are made from Si wafers of 40 nm thick SiN_x with a 5 μm thick, thermally grown SiO₂ layer sandwiched between the Si and SiN_x. Single-layer CVD graphene was grown on copper foil, several square inches in size.³⁴ After spinning on a poly(methyl methacrylate) (PMMA) support layer the copper foil was etched in iron chloride, followed by an HCl etch, and finally floated on water. The graphene was transferred onto the wafer surface containing 90 nm thick Au contact pads (Ti adhesion layer) defined by photolithography. After removal of PMMA from the graphene surface in acetone and prior to patterning, the device was heated in a rapid thermal annealer at 350 °C for an hour in 5% H₂/95% Ar in order to remove PMMA residues from the surface. Au source and drain electrodes 40 nm thick (Ti adhesion layer) were defined by electron-beam lithography, with separations of 500 nm to 1.5 μm, on top of the graphene and connected to the larger contact pads. Before further lithography, another cleaning was performed in the rapid thermal annealer under the same conditions used previously. GNRs were then patterned from the graphene sheet using electron-beam lithography on negative-tone resist HSQ and oxygen plasma etching. Raman and electron diffraction data are shown in Figures S7 and S8. TEM and STEM electron microscopy was performed with a JEOL 2010F operating at 200 kV. The current density and convergence angle of the electron beam were controlled with the condenser lenses and apertures. In STEM mode, HAADF images were acquired with a small camera length to ensure that only electrons deflected by angles larger than 50 mrad were acquired by the annular dark field detector.

Conflict of Interest: The authors declare no competing financial interest.

Acknowledgment. The authors thank C. Merchant, K. Healy, and K. Venta for preliminary work in 2009–2010 on this project, M. Sina for assistance with TEM use at Rutgers University, G. H. Han for assistance with graphene growth, and A. T. C. Johnson and his lab for useful scientific discussions. M.P. acknowledges funding from the NSF-IGERT program (Grant DGE-0221664). This work was supported by NIH Grant R21HG006313 and by the Nano/Bio Interface Center through the National Science Foundation NSEC DMR08-32802. We gratefully acknowledge use of the TEM in the NSF-MRSEC electron microscopy facility at the University of Pennsylvania and the use of the TEM facility at Rutgers University.

Supporting Information Available: Calculation of the electric potential change around the nanopore, additional AFM and TEM of devices, electron diffraction and Raman spectroscopy characterization, and bar graphs of GNR resistances before and after nanopore drilling using the TEM and STEM methods. This material is available free of charge via the Internet at <http://pubs.acs.org>.

REFERENCES AND NOTES

1. Yuan, W.; Zhou, Y.; Li, Y.; Li, C.; Peng, H.; Zhang, J.; Liu, Z.; Dai, L.; Shi, G. The Edge- and Basal-Plane-Specific Electrochemistry of a Single-Layer Graphene Sheet. *Sci. Rep.* **2013**, *3*, 2248.
2. Geim, A. K.; Novoselov, K. S. The Rise of Graphene. *Nat. Mater.* **2007**, *6*, 183–191.
3. Schedin, F.; Geim, A. K.; Morozov, S. V.; Hill, E. W.; Blake, P.; Katsnelson, M. I.; Novoselov, K. S. Detection of Individual Gas Molecules Adsorbed on Graphene. *Nat. Mater.* **2007**, *6*, 652–655.
4. Han, M.; Özyilmaz, B.; Zhang, Y.; Kim, P. Energy Band-Gap Engineering of Graphene Nanoribbons. *Phys. Rev. Lett.* **2007**, *98*, 206805.
5. Chen, Z.; Lin, Y.-M.; Rooks, M. J.; Avouris, P. Graphene Nano-Ribbon Electronics. *Phys. E (Amsterdam, Neth.)* **2007**, *40*, 228–232.
6. Özyilmaz, B.; Jarillo-Herrero, P.; Efetov, D.; Kim, P. Electronic Transport in Locally Gated Graphene Nanoconstrictions. *Appl. Phys. Lett.* **2007**, *91*, 192107.
7. Lu, Y.; Goldsmith, B.; Strachan, D. R.; Lim, J. H.; Luo, Z.; Johnson, A. T. C. High-On/Off-Ratio Graphene Nanoconstriction Field-Effect Transistor. *Small* **2010**, *6*, 2748–2754.
8. Fischbein, M. D.; Drndic, M. Sub-10 nm Device Fabrication in a Transmission Electron Microscope. *Nano Lett.* **2007**, *7*, 1329–1337.
9. Fischbein, M. D.; Drndic, M. Electron Beam Nanosculpting of Suspended Graphene Sheets. *Appl. Phys. Lett.* **2008**, *93*, 113107.
10. Lu, Y.; Merchant, C. A.; Drndic, M.; Johnson, A. T. C. In Situ Electronic Characterization of Graphene Nanoconstrictions Fabricated in a Transmission Electron Microscope. *Nano Lett.* **2011**, *11*, 5184–5188.
11. Nelson, T.; Zhang, B.; Prezhdov, O. V. Detection of Nucleic Acids with Graphene Nanopores: Ab Initio Characterization of a Novel Sequencing Device. *Nano Lett.* **2010**, *10*, 3237–3242.
12. Min, S. K.; Kim, W. Y.; Cho, Y.; Kim, K. S. Fast DNA Sequencing with a Graphene-Based Nanochannel Device. *Nat. Nanotechnol.* **2011**, *6*, 162–165.
13. Saha, K. K.; Drndic, M.; Nikolić, B. K. DNA Base-Specific Modulation of Microampere Transverse Edge Currents through a Metallic Graphene Nanoribbon with a Nanopore. *Nano Lett.* **2012**, *12*, 50–55.
14. Avdoshenko, S. M.; Nozaki, D.; Gomes da Rocha, C.; González, J. W.; Lee, M. H.; Gutierrez, R.; Cuniberti, G. Dynamic and Electronic Transport Properties of DNA Translocation through Graphene Nanopores. *Nano Lett.* **2013**, *13*, 1969–1976.
15. Gao, X. P. A.; Zheng, G.; Lieber, C. M. Subthreshold Regime Has the Optimal Sensitivity for Nanowire FET Biosensors. *Nano Lett.* **2010**, *10*, 547–552.

16. Xie, P.; Xiong, Q.; Fang, Y.; Qing, Q.; Lieber, C. M. Local Electrical Potential Detection of DNA by Nanowire–Nanopore Sensors. *Nat. Nanotechnol.* **2011**, *7*, 119–125.
17. Yang, J. K.; Cord, B.; Duan, H.; Berggren, K. K.; Klingfus, J.; Nam, S.-W.; Kim, K.-B.; Rooks, M. J. Understanding of Hydrogen Silsesquioxane Electron Resist for Sub-5-nm-Half-Pitch Lithography. *J. Vac. Sci. Technol. B* **2009**, *27*, 2622–2627.
18. Nam, S.-W.; Rooks, M. J.; Berggren, K. K.; Yang, J. K.; Kim, K.-B.; Lee, M.-H.; Kim, H.-M.; Yoon, D. Y.; Sim, J. H. Contrast Enhancement Behavior of Hydrogen Silsesquioxane in a Salty Developer. *J. Vac. Sci. Technol. B* **2009**, *27*, 2635–2639.
19. Chen, J. H.; Jang, C.; Adam, S.; Fuhrer, M. S.; Williams, E. D.; Ishigami, M. Charged-Impurity Scattering in Graphene. *Nat. Phys.* **2008**, *4*, 377–381.
20. Pirkle, A.; Chan, J.; Venugopal, A.; Hinojos, D.; Magnuson, C. W.; McDonnell, S.; Colombo, L.; Vogel, E. M.; Ruoff, R. S.; Wallace, R. M. The Effect of Chemical Residues on the Physical and Electrical Properties of Chemical Vapor Deposited Graphene Transferred to SiO₂. *Appl. Phys. Lett.* **2011**, *99*, 122108.
21. Lin, Y.-C.; Lu, C.-C.; Yeh, C.-H.; Jin, C.; Suenaga, K.; Chiu, P.-W. Graphene Annealing: How Clean Can It Be? *Nano Lett.* **2011**, *12*, 414–419.
22. Lo, C. J.; Aref, T.; Bezryadin, A. Fabrication of Symmetric Sub-5 nm Nanopores Using Focused Ion and Electron Beams. *Nanotechnology* **2006**, *17*, 3264–3267.
23. Yang, J.; Ferranti, D. C.; Stern, L. A.; Sanford, C. A.; Huang, J.; Ren, Z.; Qin, L.-C.; Hall, A. R. Rapid and Precise Scanning Helium Ion Microscope Milling of Solid-State Nanopores for Biomolecule Detection. *Nanotechnology* **2011**, *22*, 285310.
24. Venta, K.; Shemer, G.; Puster, M.; Rodríguez-Manzo, J. A.; Balan, A.; Rosenstein, J. K.; Shepard, K.; Drndic, M. Differentiation of Short, Single-Stranded DNA Homopolymers in Solid-State Nanopores. *ACS Nano* **2013**, *7*, 4629–4636.
25. Meyer, J. C.; Eder, F.; Kurasch, S.; Skakalova, V.; Kotakoski, J.; Park, H. J.; Roth, S.; Chuvilin, A.; Eychusen, S.; Benner, G.; *et al.* Accurate Measurement of Electron Beam Induced Displacement Cross Sections for Single-Layer Graphene. *Phys. Rev. Lett.* **2012**, *108*, 196102.
26. Banhart, F.; Kotakoski, J.; Krasheninnikov, A. V. Structural Defects in Graphene. *ACS Nano* **2011**, *5*, 26–41.
27. Childres, I.; Jauregui, L. A.; Foxe, M.; Tian, J.; Jalilian, R.; Jovanovic, I.; Chen, Y. P. Effect of Electron-Beam Irradiation on Graphene Field Effect Devices. *Appl. Phys. Lett.* **2010**, *97*, 173109.
28. Chen, J.-H.; Cullen, W.; Jang, C.; Fuhrer, M.; Williams, E. Defect Scattering in Graphene. *Phys. Rev. Lett.* **2009**, *102*, 236805.
29. Banhart, F. Irradiation Effects in Carbon Nanostructures. *Rep. Prog. Phys.* **1999**, *62*, 1181–1221.
30. Egerton, R. F.; Li, P.; Malac, M. Radiation Damage in the TEM and SEM. *Micron* **2004**, *35*, 399–409.
31. Williams, D. B.; Carter, C. B. *Transmission Electron Microscopy*; Springer: Berlin, 2009.
32. Howitt, D. G.; Chen, S. J.; Gierhart, B. C.; Smith, R. L.; Collins, S. D. The Electron Beam Hole Drilling of Silicon Nitride Thin Films. *J. Appl. Phys.* **2008**, *103*, 024310.
33. Kim, H.-M.; Lee, M.-H.; Kim, K.-B. Theoretical and Experimental Study of Nanopore Drilling by a Focused Electron Beam in Transmission Electron Microscopy. *Nanotechnology* **2011**, *22*, 275303.
34. Luo, Z.; Lu, Y.; Singer, D. W.; Berck, M. E.; Somers, L. A.; Goldsmith, B. R.; Johnson, A. T. C. Effect of Substrate Roughness and Feedstock Concentration on Growth of Wafer-Scale Graphene at Atmospheric Pressure. *Chem. Mater.* **2011**, *23*, 1441–1447.